INORGANIC BOVINE-DERIVED HYDROXYAPATITE MATRIX/P15 PROTEIN AS A BONE GRAFT SUBSTITUTE FOR PERIODONTAL DEFECT REPAIR OF WISTAR RATS MODEL

W. H. Xu, L. F. Yin, M. L. Zhou and X.L. Luo*

Department of Periodontics, Hunan University of Chinese Medicine Affiliated Changsha Stomatological Hospital, Changsha, 410004, Hunan, China.
*Corresponding author's Email: luoxiaoliang2023@yeah.net

ABSTRACT

This study was developed to evaluate efficacy of inorganic bovine-derived hydroxyapatite matrix (ABM) plus P15 protein (ABM/P15) as a bone graft material for periodontal defect repair in a rat model. Fresh bovine-derived bone (BDB) served as raw material, and single solvent method was adopted to obtain ABM. The acquisition of ABM from BDB powder was evaluated at different heating temperatures. After dissolving, P15 was added to ABM, and the ABM/P15 composite material was obtained through mixing, heating, and drying processes. Molecular structure and elemental compositions were analyzed using Fourier Transform Infrared Spectroscopy (FTIR) and X-Ray Diffraction (XRD), respectively. Furthermore, 30 male Wistar rats were selected to establish a periodontal disease (PD) model and were randomly assigned to a control group (PD repaired with ABM) and an observation group (PD repaired with ABM/P15), with 15 rats in each. Bone regeneration status was analyzed employing micro-CT 3D reconstruction at postoperative 1, 2, and 3 months. Hematoxylin and eosin (H&E) staining visualized the morphological changes in periodontal tissues. Additionally, inflammatory cell changes were detected by Masson's trichrome (MT) staining, and cysteinyl aspartate specific proteinase-3 (caspase-3) and B-cell lymphoma-2 (Bcl-2) levels were examined by western blotting. FT-IR analysis showed consistent molecular structures of ABM, synthetic hydroxyapatite, and ABM/P15. XRD results revealed that ABM/P15 exhibited a weak crystalline state. The periodontal tissue recovery in the observation group was markedly better than in the control group at 1, 2, and 3 months' post-surgery, with the bone regeneration height (ABRH) being notably higher in the observation group ($P \leq 0.05$). H&E and MT staining results revealed that the inflammatory reactions in the control group remained higher than that in the observation group at various time points. Western blotting analysis showed no statistically significant differences in caspase-3 and Bcl-2 expression levels in the periodontal tissue between control and observation rats at 1, 2, and 3 months' post-surgery ($P > 0.05$). ABM/P15 composite material effectively promotes periodontal tissue regeneration in an animal PD model, without inducing significant inflammatory reactions, demonstrating good animal experimental outcomes and safety.

Key words: Inorganic bovine-derived hydroxyapatite matrix; P15 protein; periodontal defect; rat model.

https://doi.org/10.36899/JAPS.2026.5.0112 Published first online June, 22, 2026

INTRODUCTION

Periodontal defects are common and frequently occurring conditions in the field of dentistry, with common causes including periodontitis, trauma, caries, and other chronic periodontal diseases (PDs), all of which severely affect patients' quality of life (Yang *et al*., 2024; Chen *et al*., 2024). The repair of these defects involves not only the regeneration of teeth and periodontal tissues but also considerations regarding the biocompatibility, mechanical properties, and bioactivity of the repair materials. Consequently, the development of new bone graft substitutes has become one of the research hotspots (Elfana and Elbehwashy, 2022). Autologous bone grafting (Elgend *et al*., 2023) and allogeneic bone grafting (Venkataiah *et al*., 2019) are traditional treatment methods, but they have the issue of donor deficiency (Grün *et al*., 2023). Hence, another approach is urgently needed.

Bovine-derived hydroxyapatite (BHA), serving as an alternative component in composite materials, consists of 93% hydroxyapatite and 7% β-tricalcium phosphate (Budiatin *et al.*, 2022). Inorganic bovine hydroxyapatite matrix (ABM) is a common xenograft in periodontal treatment (Sah *et al*., 2025). ABM is widely used due to its excellent biocompatibility, good osteoinductivity, and ability to promote bone formation (Babayiğit *et al*., 2023; Yao *et al.*, 2022). However, pure hydroxyapatite still has limitations in bone repair, which has prompted researchers to study enhancing

BHA function by incorporating bioactive molecules such as peptides and growth factors. Costa *et al.* mixed hydroxyapatite with polyetheretherketone (PEEK) for bone repair (Costa *et al.*, 2024). However, these studies lack a systematic evaluation of their adaptability to the periodontal microenvironment.

P15 plus inorganic matrix (such as hydroxyapatite or bioactive glass) greatly improved its stability and achieved a sustained release effect (Axelsen *et al*., 2019; Ureiro-Cueto *et al*., 2024). P15 protein acts as a bioactive molecule in bone regeneration (Chan *et al.*, 2021; Li *et al.*, 2023). P15 protein regulates the osteogenesis of bone marrow mesenchymal stem cells by binding to cell surface receptors (Wang *et al.*, 2022). The binding of P15 protein with inorganic materials can enhance the bone repair effect in periodontal defect repair, promoting new bone formation and accelerating tissue healing (Atieh *et al*., 2021). Previous studies combined P15 protein with ABM to form ABM/P15 composites, which proved its ability to significantly enhance bone bonding performance in spinal fusion experiments (Jacobsen *et al.*, 2020; Andresen *et al.*, 2022). Although ABM/P15 composite has excellent biocompatibility and bioactivity, its efficacy in periodontal defect restoration is still controversial. Some studies show that its long-term efficacy and safety are uncertain and need further evaluation.

Based on the above content, this work aimed to establish a rat periodontal defect model and comprehensively evaluate the effectiveness and safety of ABM/P15 protein as a bone graft substitute for repairing periodontal defects. Although the existing research explored the composite strategy involving BHA and other materials, there is still a lack of systematic research on the dual roles of P15 protein in promoting osteogenesis and anti-inflammation in periodontal defect repair. Animal models have become an indispensable part of research on oral biomaterials. Gani et al. adopted a Wistar rat femoral bone defect model for assessment of bone repair effect of BMP-2 carrier, and it turned out that the carrier accelerated new bone formation and defect healing (Gani *et al*., 2022). Another study, using rat models to evaluate the effectiveness of various biomaterials in periodontal defect repair, showed that composite materials promoted new bone formation (Xu *et al*., 2023). Wang *et al*. (2022) also used the rabbit bone defect model to explore the role of P15 protein in promoting bone healing, which proved that P15 protein notably enhanced bone repair (Wang *et al*., 2022).

This study aimed to fabricate a composite material with good biocompatibility and osteoinductivity using ABM with P15 protein. Compared with previous studies, this study systematically analyzed the bone regeneration anti-inflammatory synergistic mechanism of ABM/P15 in periodontal defects for the first time, and optimized the degradation rate based on biomimetic design to meet clinical needs. Through experimental validation using a rat model, this study aimed to provide a novel alternative bone graft material for the clinical treatment of periodontal defects.

MATERIALS AND METHODS

Preparation of ABM/P15: Fresh bovine-derived bone (BDB) samples (Red Star Market, Changsha, Hunan, China) were first subjected to preliminary processing to remove soft tissue, periosteum, and bone marrow, eliminating non-bone components. The bone was then washed to remove blood, cut into small pieces, and heated in water at 70-80°C for approximately 4 hours. After cooling, excess fat was removed, followed by defatting with solvent gasoline (Hubei Xinrunde Chemical Co., Ltd., China) through soaking and washing, and thoroughly rinsed with warm water. After natural air drying, the bone pieces were placed in a 40°C oven (Wujiang Dongwu Oven Equipment Co., Ltd., China) and dried for 50 hours. The resulting bone pieces were processed in a high-speed multifunctional grinder (Shanghai Sheyan Instrument Co., Ltd., China) for 5 minutes to obtain BDB powder. Meanwhile, 1-ethyl-3-methylimidazolium bromide ([Bmim]Br) ionic liquid was synthesized by mixing N-methylimidazole (Shanghai Kaiyin Chemical Co., Ltd., China) and ethyl bromide (Shanghai Kaiyin Chemical Co., Ltd., China) in a 1:1.3 molar ratio, followed by stirring and refluxing at 60°C for 4 hours. After the reaction, the mixture was washed with ethyl acetate (Shanghai Kaiyin Chemical Co., Ltd., China) and purified using a rotary evaporator (Zhengzhou Huachen Instrument Co., Ltd., China) to remove impurities. The final ionic liquid, [Bmim]Br, was obtained by vacuum drying. Next, an appropriate amount of BDB powder was mixed with [Bmim]Br ionic liquid in a 1:10 ratio and placed into a three-neck round-bottom flask (KIMAX, USA), which was then heated in a water bath to various temperatures (80, 100, 140, 180, 200, 220, 240, 260°C), while being stirred with a magnetic stirrer (Shanghai Sheyan Instrument Co., Ltd., China) for 5 hours. The mixture was then filtered through a copper mesh (Anping County Guanwo Wire Mesh Products Co., Ltd., China) to separate the undissolved bone materials, followed by washing and drying. Equal volumes of dichloromethane (Shanghai Kaiyin Chemical Co., Ltd., China) were added to the filtrate, and the solution was further filtered in stages through regular filter paper and 450, 220 nm filter membranes (Zibo Dongqiang Membrane Technology Co., Ltd., China), respectively. The resulting filter cake was rinsed with distilled water at 60°C (Shanghai Kaiyin Chemical Co., Ltd., China) to remove any residual ionic liquid and then dried in a 60°C oven to obtain ABM powder. The mass of ABM was recorded, and the dissolution of BDB powder and the yield of ABM were compared at different temperatures. For the preparation of the P15 protein solution, P15 protein powder was added to physiological saline (Shanghai Kaiyin Chemical Co., Ltd., China) to achieve the desired concentration, and the solution was filtered to remove any undissolved P15 protein powder. Dry ABM particles

were placed in a beaker and the prepared P15 protein solution was slowly applied while stirring thoroughly to ensure uniform adhesion of P15 protein to the surface of the ABM particles. Stirring lasted for 5 hours until a uniform ABM/P15 composite was formed. Subsequently, the composite material was dried in a 40°C oven for 4 hours to obtain a solid composite material. Finally, grind and process the ABM/P15 composite material into the desired shape and size, and then sterilize it. The obtained ABM/P15 composite material is uniform and sturdy, meeting specific application requirements while maintaining sterility.

Characterization of materials: ABM, synthetic hydroxyapatite, and ABM/P15 underwent molecular structure analysis employing Fourier Transform Infrared Spectroscopy (FT-IR) (Arcoptix, Beijing Haikesirui Optoelectronics Instrument Co., Ltd., China) (Diansari *et al*., 2025). The following parameters were set: resolution = 4 cm^{-1}, scanning frequency = 20, and range = 400 cm^{-1} to 4000 cm^{-1}. X-ray Diffraction (XRD) (Xu *et al*., 2023) instrument (Dandong Tongda Technology Co., Ltd., China) was employed to analyze the elemental compositions (scanning speed =4°/min, step size =0.05°, range =5°~85°).

Establishment of periodontal defect rat model: Thirty-six-week-old specific pathogen-free (SPF) male Wistar rats (body weight=200~300 g, Guangdong Mingzhu Biotechnology Co., Ltd., China) in good health were utilized. All mice underwent a health assessment to ensure that there were no gum or tooth related diseases. All experiments were approved by Ethics Committee of Hunan University of Chinese Medicine Affiliated Changsha Stomatological Hospital, and in accordance with the Guide for the Care and Use of Laboratory Animals published by the United States National Institutes of Health.

All SPF rats were acclimated to the environment of temperature (22±2℃), relative humidity (50±10%) and 12 hours light/dark cycle for one week, and then they were divided into groups according to the standard of no more than five rats per cage. Subsequently, the PD model was constructed (Zhang *et al.*, 2025). Firstly, anesthesia was induced by intravenous injection of 70 - 120 mg/kg of phenobarbital sodium (Nanjing Jinhaiwei New Materials Co., Ltd., China). Basic periodontal treatment was performed to ensure uniform baseline conditions among all rats. One week after the baseline treatment, the PD surgery was conducted. The second molar in the upper molar region was selected for the procedure. Flap elevation and deboning were used to make PD. The depth of PD was 3 mm and the width was 2 mm, and the width was based on the buccal side of the exposed root. The periodontal ligament on the root surface was removed, and a part of alveolar bone was scraped off gently with a dental scaler (UK). Using a small ball drill with a diameter of 1 mm (Shanghai Sheyan Instrument Co., Ltd., China), a shallow indentation with a depth of 0.4 mm was made on the root surface at the bottom of the defect as a marker of PD locus. The defect area was also gently stimulated to promote the inflow of fresh blood. This method established a stable and controllable periodontitis (PD) model in the maxillary molar region of rats, which facilitated the subsequent evaluation of the repair effects of different materials in periodontal defects.

Grouping and treatments: Thirty male rats were randomly rolled into control group and observation group, with 15 rats in each group. In the control group, ABM material was only inserted into PD site for repair. In the observation group, ABM/P15 was implanted in PD site for repair. After implantation, the gingival flap was repositioned and sutured. Three days after operation, all rats received anti-infective preventive treatment by intramuscular injection of streptomycin (Sigma Corporation, USA) at a dose of 8×10^4 U/day. This preventive treatment was performed once a day to minimize the risk of postoperative infection.

micro-CT scanning and quantification of alveolar bone regeneration (Sindhusha *et al*., 2024)**:** Five experimental rats from each group were anesthetized 1, 2, and 3 months after the repair operation. Rats were perfused through the common carotid artery and fixed with 4% paraformaldehyde solution (Nanjing Jinhaiwei New Materials Co., Ltd., China). Two groups of rat mandibles containing PD sites were extracted. Initially, macroscopic evaluation was conducted to visualize the recovery of periodontal tissue, including gingival redness, swelling, suture retention, exposure or extrusion of graft materials, and the presence of pus. The tissue blocks closest to the implanted teeth were taken from all experimental rats for micro-CT (Scanco, Switzerland) analysis to evaluate bone regeneration status. The scanning parameters of micro-CT were as follows: voltage =50 kVp, current =150 A, and time interval =180 ms. The acquired images were reconstructed and analyzed using the Scanco Evaluation Program software (Scanco Medical AG, Switzerland). The primary outcome measure, alveolar bone regeneration height (ABRH), was used to quantify new bone formation within the defect. In a sagittal section through the center of the defect, ABRH was defined as the vertical distance from the baseline of the surgically created defect to the most coronal point where a continuous mineralized bone bridged the defect. All measurements were performed by two independent, blinded examiners within a consistent region of interest (ROI) encompassing the defect site, and the average value for each sample was recorded.

Hematoxylin and eosin (H&E) (Özer *et al*., 2023) **and Masson's trichrome (MT) stainings** (Sindhusha *et al*., 2024)**:** Specimens were decalcified, dehydrated, embedded in paraffin, and sliced, and then stained with H&E and MT.

Firstly, xylene and gradient ethanol (100%, 95%, and 70%) (Sigma Company, USA) were used in turn, and each solution was carried out for 2 rounds, each time for 5 minutes. In the second step, 3% acetic acid (Sigma Company, USA) was applied for 3 minutes, then Azur B solution (Sigma Company, USA) with pH=2.5 was utilized for 40 minutes, and then ethyl acetate (Shanghai, Kaiyin Chemical Co., Ltd., China) was applied for 2 minutes. In step 3, hematoxylin solution (Sigma Company, USA) was utilized for 5 minutes. In the fourth step, eosin (Sigma Corporation, USA) was added for 15 seconds, followed by 95% and 100% ethanol, each with 30 dips and repeated 2 times, and xylene for 1 minute, twice. Next, the slides (Thermo Fisher Scientific, USA) were sealed with 80 μL cover slip (Sigma Corporation, USA) adhesive and dried. Note: the distilled water was employed for a 2-minute rinse after both the first and second steps.

MT staining: in the first step, the procedure was the same as in the HE staining. In the second step, Weigert's iron hematoxylin (Sigma Corporation, USA), Biebrich Scarlet-Acid Fuchsin solution (Sigma Corporation, USA), Phosphotungstic/Polyphomolybdic acid solution (Sigma Corporation, USA), and Aniline blue solution (Sigma Corporation, USA) were sequentially added, each shaken on a room-temperature shaker for 2 to 5 minutes. Prior to adding each new solution, a rinse with distilled water for 1 to 5 minutes was performed. In the third step, 70%, 80%, and 90% ethanol were used for 20 dips, followed by two rounds of 5-minute incubations in 100% ethanol and xylene. At the end, the slides were sealed with 80 μL cover slip adhesive and dried.

It was evaluated whether there was an inflammatory reaction in tissues at 1, 2, and 3 months after the operation. The results of tissue sections were analyzed with a digital imaging device (QImaging, Canada) at a magnification of 4 times.

Western blotting: After dyeing, the remaining tissue samples were processed and analyzed by Western blotting to evaluate the potential toxic effects of two kinds of repair materials on periodontal tissues. Initially, the tissue specimens were minced, digested, and centrifuged to collect the supernatant for protein quantification. Subsequently, proteins were separated using SDS-PAGE, and the proteins were transferred to a PVDF membrane (IPVH00010 Millipore, USA). The membrane was washed with TBST buffer (Thermo Fisher Scientific, USA), blocked with 5.0% non-fat dry milk (Sigma Corporation, USA) for 1 hour at room temperature, and then incubated overnight at 4°C with the following primary antibodies: rabbit anti-cysteine-aspartic acid protease 3 (caspase-3) (1:1000; Abcam, USA) and rabbit anti-B-cell lymphoma-2 (Bcl-2) (1:500; Abcam, USA). After membrane washing (5 minutes) with repeated 3 times, the secondary antibody (1:5000, goat anti-rabbit IgG, Santa Cruz, USA) was added for a further incubation for 40 minutes. Subsequently, chemiluminescence detection using an enhanced chemiluminescence reagents (ECL) (Sigma Corporation, USA) was implemented, and the analysis was conducted with β-actin (Sigma Corporation, USA) as the internal reference protein.

Statistical analysis: Employing *SPSS 19.0*, all data were presented as $x' \pm s$ (Where x' represents the mean value and s represents the standard deviation). The t-test analyzed the differences between two groups, while one-way analysis of variance was utilized for comparisons among multiple groups. $P \leq 0.05$ meant statistically significant differences.

RESULTS

Dissolution of BDB powder and ABM mass at various temperatures: Dissolution of BDB powder (Figure 1A) and changes in ABM mass (Figure 1B) were analyzed at temperatures of 120°C, 140°C, 160°C, 180°C, 200°C, 220°C, 240°C, and 260°C. Both the dissolved mass of BDB powder and the ABM mass gradually increased with rising temperature (from 0.49 g-1.37 g). At 220°C, both the dissolution of BDB powder and the ABM mass had a drastic increase, showing a similar trend.

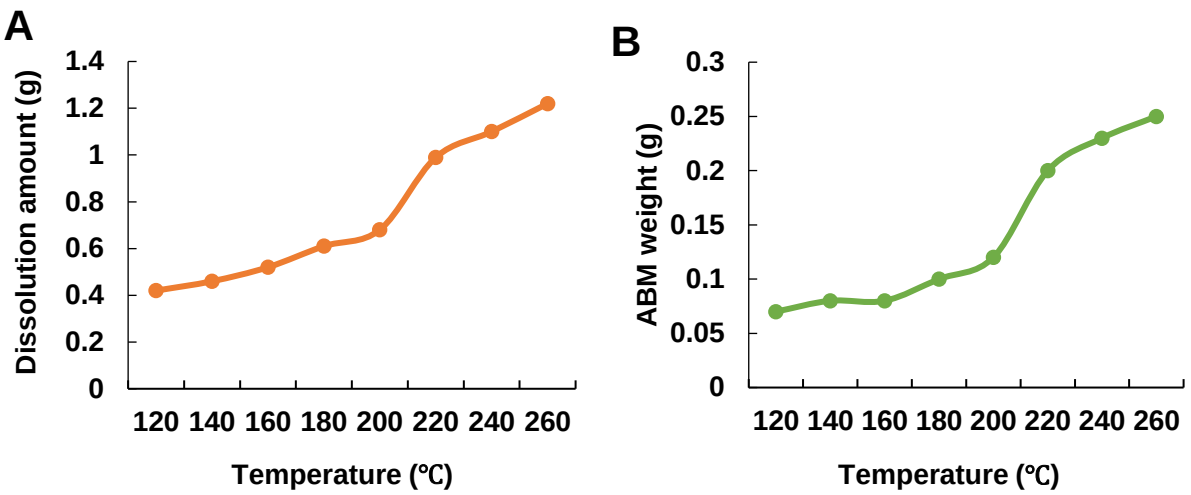

Figure 1: changes in dissolution of BDB powder (A) and ABM mass (B) at various temperatures.

Characterization of synthetic hydroxyapatite: Figure 2 displays the FT-IR spectral characteristics of the materials in each group. All samples exhibited water absorption peaks around ~3,450 cm^{-1} and ~1,650 cm^{-1} and characteristic absorption peaks of hydroxyapatite at 1,000^{-1}, 100 cm^{-1} (PO_4^{3-} stretching vibration) and 500-700 cm^{-1} (PO_4^{3-} bending vibration). Notably, the ABM/P15 composite group showed a distinct C=O stretching vibration peak at 1,522 cm^{-1} ($P \leq 0.05$), confirming the successful loading of P15 protein.

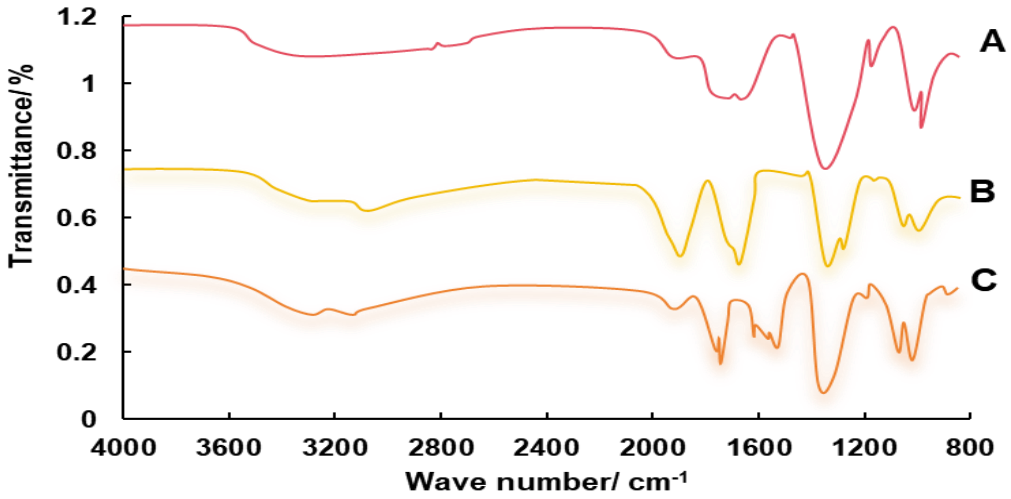

Figure 2: FT-IR results of ABM (A), synthetic hydroxyapatite (B), and ABM/P15 (C).

Figure 3A-C depicted the XRD results of ABM, synthetic hydroxyapatite, and the ABM/P15, respectively. The characteristic peaks of them were evident in the figures. In comparison with synthetic hydroxyapatite, ABM exhibited stronger diffraction peaks and a more well-defined crystallinity. In contrast to ABM, the ABM/P15 presented no significant alteration in the crystalline phase of ABM itself during the composite process. However, the crystallinity of the composite material was reduced.

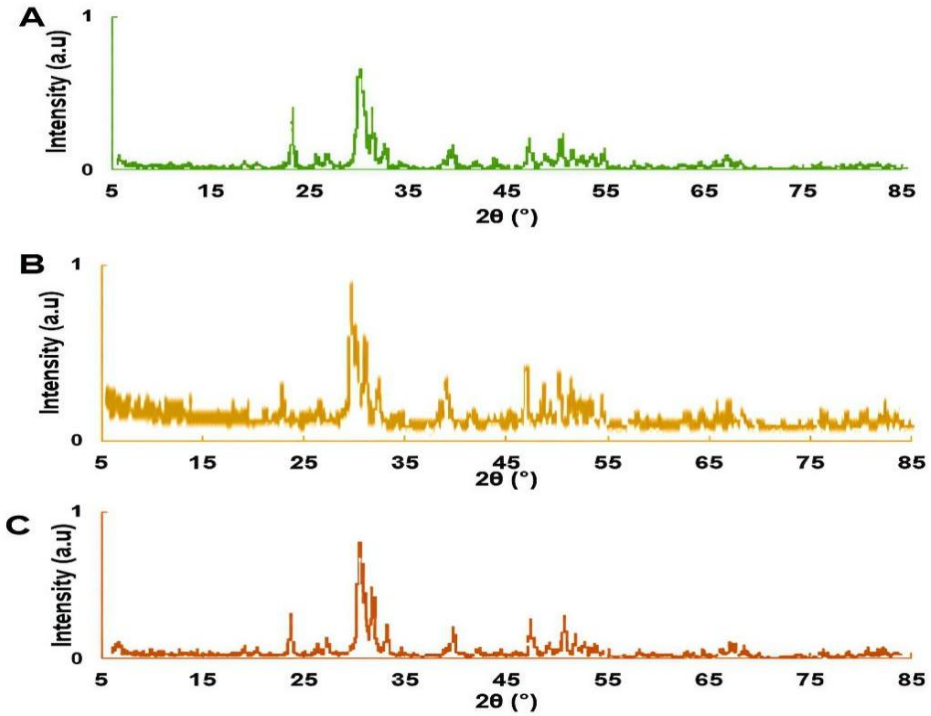

Figure 3: XRD results of ABM (A), synthetic hydroxyapatite (B), and ABM/P15 (C).

ABRH results: Comparison showed that the highest ABRH in the observation group at 1-month post-surgery ((2.08 ± 0.54) mm vs. (0.76 ± 0.25) mm), 2 months' post-surgery ((3.67 ± 0.48) mm vs. (1.01 ± 0.57) mm), and 3 months post-surgery ((4.55 ± 0.49) mm vs. (1.77 ± 0.44) mm) were significantly higher than those in the control group ($P \leq 0.05$) (Figure 4).

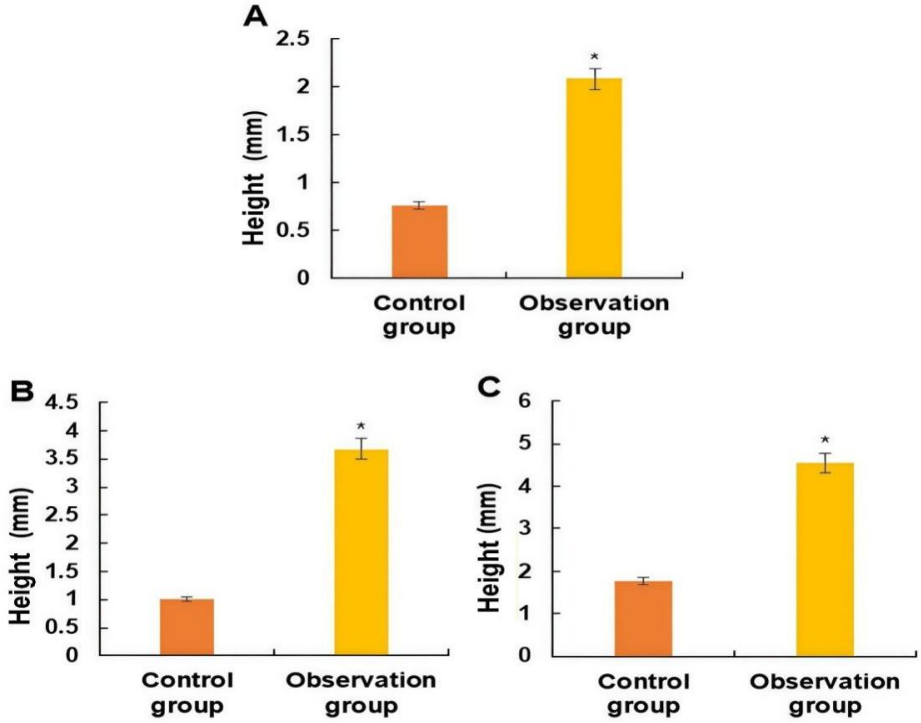

Figure 4: Comparison on the highest ABRH at postoperative 1 (A), 2 (B), and 3 (C) months. * Compared with control group, $P \leq 0.05$.

Tissue staining results: Figure 5 presented the results of H&E staining. By 1 month after surgery, both groups showed the presence of inflammatory cells. In the control group, the density of inflammatory cells was significantly higher than that in the observation group. By 2 months after surgery, there are residual inflammatory cells in the control group, and the overall degree of inflammation is still higher than that in the observation group. By 3 months after surgery, with a small number of scattered inflammatory cells observed in the control group, but tissue maturity was slightly lower than that in the observation group.

The MT staining results are shown in Figure 6. At 1 month postoperatively, inflammatory cells were observed in both groups, with a higher density of inflammatory cells in the control group. Meanwhile, collagen deposition was more pronounced in the observation group. At 2 months postoperatively, inflammatory cells were significantly reduced in both groups, while collagen deposition increased. However, compared with the control group, collagen deposition was more evident in the observation group. By 3 months postoperatively, almost no inflammatory cells were observed in the observation group, whereas a small number of residual inflammatory cells still remained in the control group. In addition, the observation group exhibited more abundant collagen deposition.

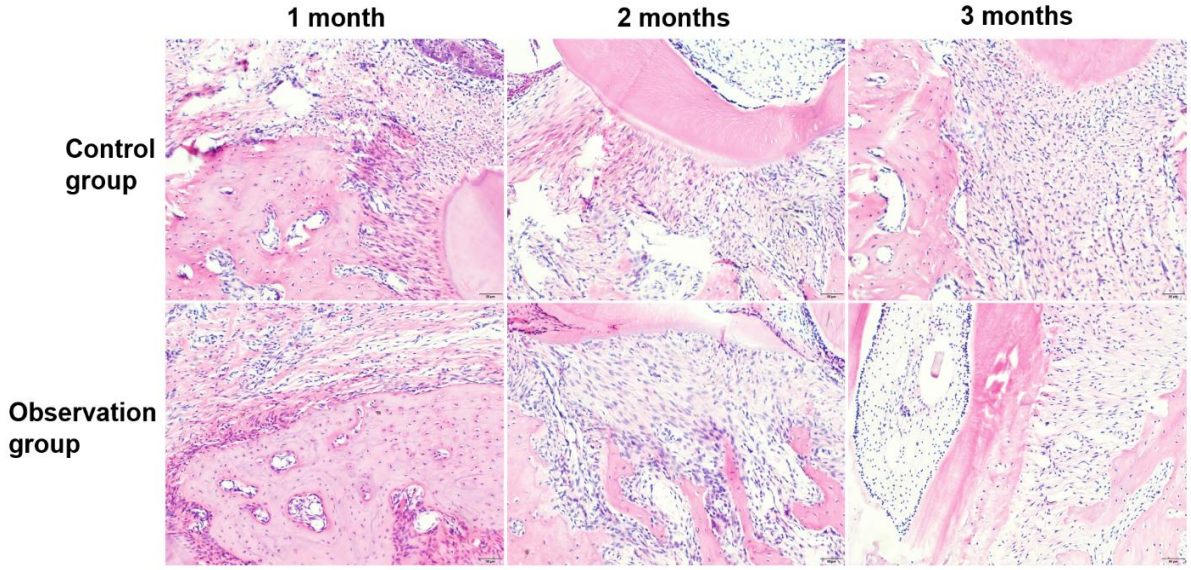

Figure 5: HE staining results in observation group and control group (100×).

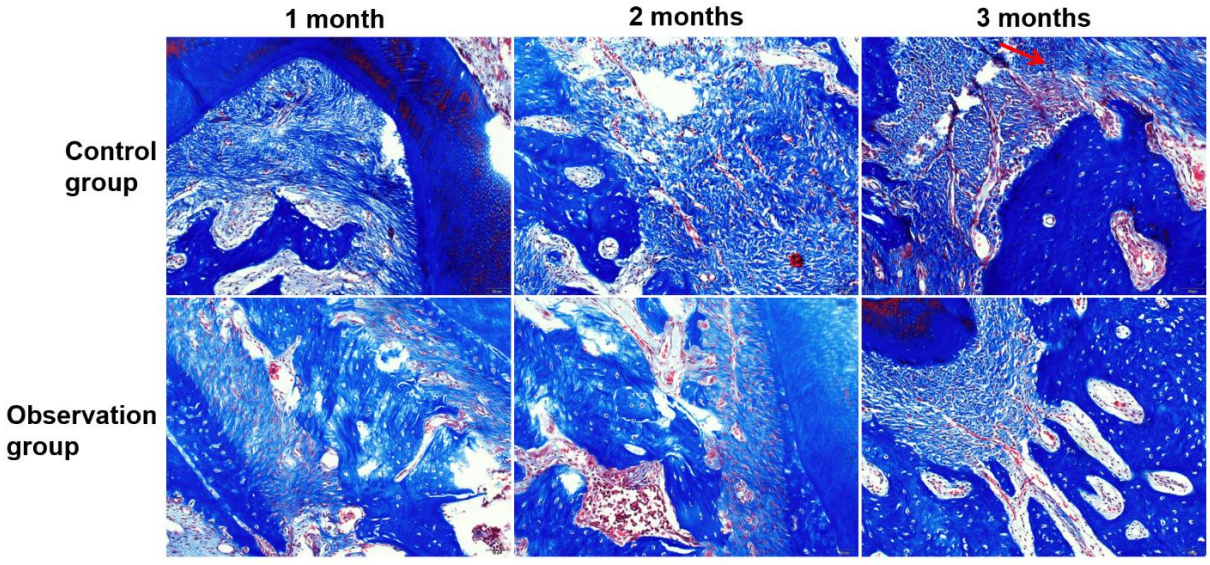

Figure 6: MT staining results in observation group and control group (100×).

Western blotting results: The study used western blotting to assess the levels of caspase-3 and Bcl-2 in the dental tissue of control group and observation group at 1, 2, and 3 months post-surgery (Figure 7). The comparative results indicated that there were no significant differences in the levels of caspase-3 and Bcl-2 in the dental tissue between the two groups at any time point ($P > 0.05$). Caspase-3 or Bcl-2 levels were observed with no considerable difference at these time points.

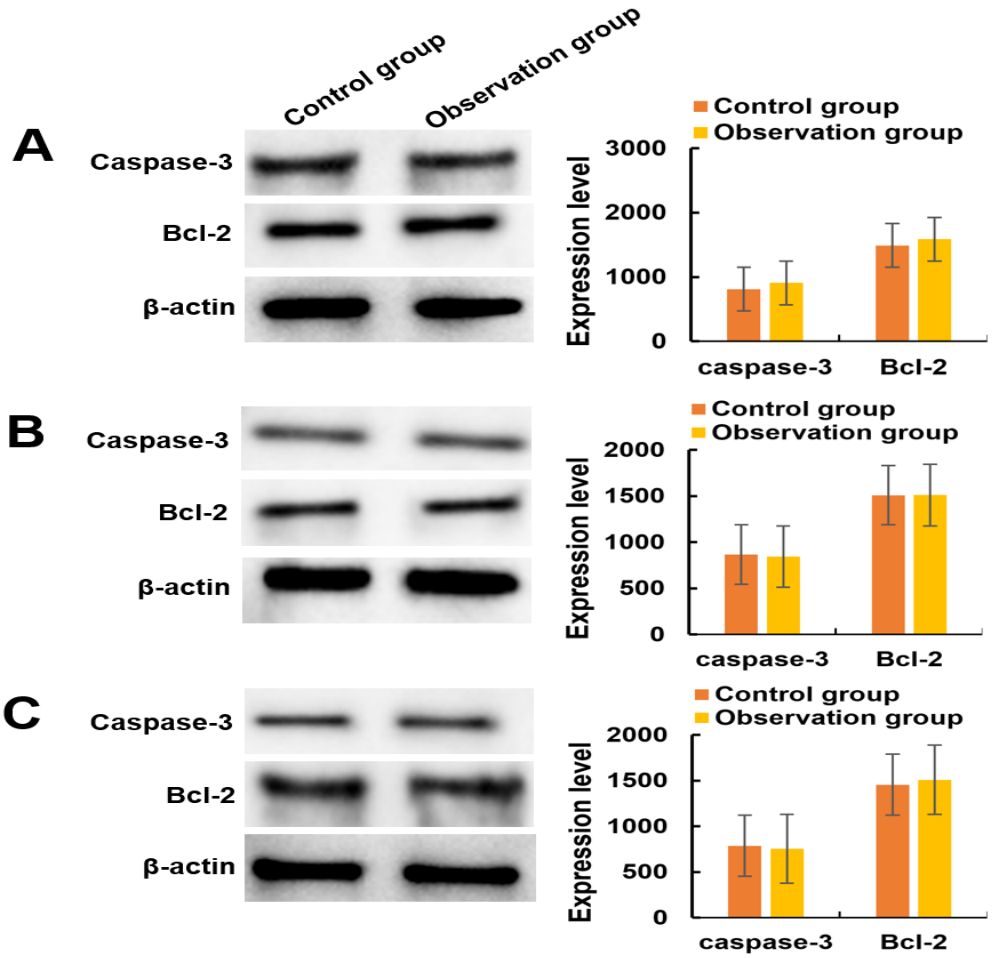

Figure 7: Western blotting results of caspase-3 and Bcl-2 at 1 month (A), 2 months (B), and 3 months (C) post-surgery.

DISCUSSION

The application of ABM combined with P15 protein in periodontal defect repair was discussed by using rat model. The results showed that ABM/P15 composite not only effectively promoted bone regeneration, but also markedly accelerated the process of periodontal tissue repair, showcasing superior therapeutic effect.

First, with the increase of temperature, the dissolution degree of BDB powder and ABM mass gradually increased, and a significant enhancement was observed at 220°C. This enhancement is related to the interaction between [Bmim]Br ionic liquid and collagen in BDB and ABM (Iqbal *et al.*, 2018). [Bmim]Br ionic liquid promotes the dissolution of bovine bone powder through its interaction with hydrogen bonds at 120-160°C, enhancing the solubility of bovine bone powder (Minim *et al.*, 2023; Akindoyo *et al.*, 2019). Further characterization results indicated that the infrared spectrum of synthesized hydroxyapatite was similar to that of ABM, especially at the absorption peak of CO_3^{2-} carbonate ions, implying a highly similar chemical composition. The similarity between ABM and human bone tissue had also been confirmed (Bergara-Muguruza *et al.*, 2021). The FT-IR spectrum of ABM/P15 composite showed an additional C=O stretching vibration peak, which indicated that P15 protein successfully attached to the surface of ABM

and reacted with Ca^{2+}, and confirmed the formation of ABM/P1 penta-complex. XRD analysis indicated that the crystalline phase of ABM/P15 composite remained stable, but the crystallinity decreased slightly (Yukna *et al*., 2000), which was consistent with the weak crystalline state of hydroxyapatite crystals found in human bones (Mohanram *et al*., 2020). Hence, ABM/P15 composite is of low crystallinity, closer to natural biological bone.

Micro-CT analysis of bone regeneration at various time points after surgery showed that the bone regeneration height of the ABM/P15 composite material group was significantly better than that of the control group at all-time points. Hence, P15 protein promotes bone regeneration, especially in the repair of periodontal defects. This effect is due to the β-corner structure formed by GIAG residues in P15 protein and the cell binding active peptide composed of two β-chains, which can promote cell adhesion and enhance cell differentiation and osteogenesis (Zhang *et al*., 2017; Guo *et al*., 2023; Jann *et al*., 2020). ABM contains calcium carbonate, and its three-dimensional structure is helpful for cell infiltration (Klassmann *et al*., 2023). It was pointed out that ABM/P15 composite can promote the synthesis of BMP-2 in osteoblasts and stimulate the activity of alkaline phosphatase in bone marrow cells (Elabbasy *et al*., 2023). In addition, porous hydroxyapatite can improve bone graft performance and reduce the risk of infection (Amelot *et al*., 2021). Our research found that the inflammatory cells observed at any time point in the experiment process can be ignored, which indicates that ABM/P15 material has good biocompatibility and low inflammatory reaction. Western blotting analysis showed that Caspase-3 and Bcl-2 levels did not exhibit considerable increases at various time points. This study showed that fibroblasts are abundant in dental pulp. They regulate immune response and secrete growth factors to promote dentin repair, angiogenesis and nerve growth, and play an important role in tooth tissue regeneration (Chang *et al.*, 2023). Caspase-3 and Bcl-2 are key proteins in the process of cell apoptosis, and their increased levels indicate enhanced apoptosis (Yang *et al*., 2023; Badaro-Garcia *et al*., 2023). Some studies proposed that caspase-3 and Bcl-2 promote the apoptosis of dental fibroblasts and indirectly affect the restoration of tooth defects (Wang *et al*., 2021). Loenen *et al*. also confirmed that P15 protein has no adverse effect on the health of organisms (Loenen *et al*., 2022). Hence, it was concluded that ABM/P15 demonstrated good clinical regenerative effects and safety in treating periodontal defects. Mishra *et al*. proposed that ABM/P15 could enhance the migration of fibroblasts and their adhesion to bone graft materials, thus improving periodontal regeneration (Mishra *et al*., 2019). Shaikh *et al*. confirmed in their study that ABM/P15 provides better clinical attachment levels (CAL), effectively assisting in periodontal regeneration of intrabony defects in routine periodontal surgeries (Shaikh *et al*., 2020).

Although this study has confirmed the significant periodontal regenerative ability and safety of ABM/P15 composite material in a rat model, there are still several limitations. The long-term degradation rate of the material and the balance of bone remodeling remain unclear. The current model does not simulate pathological microenvironments such as those in diabetic patients or those with osteoporosis. The sustained-release kinetics of P15 protein and its dynamic interaction with the host immune system still need to be further elucidated. Therefore, future research will focus on the following points. First, future research should establish periodontal defect models in large animals (such as dogs/pigs) and integrate clinical imaging evaluation to evaluate the integration of materials in complex anatomical structures. Second, future research should develop a temperature-responsive P15 controlled release system (for example, based on 220°C trigger release) to accurately adjust the osteogenic signal in space and time. Thirdly, future research should combine single cell sequencing technology to reveal the epigenetic mechanism of ABM/P15 regulating the fate of periodontal stem cells (such as osteogenesis-angiogenesis coupling). These breakthroughs will promote the transformation of ABM/P15 from laboratory to clinical practice, and provide innovative tools for personalized periodontal regeneration treatment.

Conclusion: The present study confirmed that, compared with the use of anorganic bovine-derived hydroxyapatite matrix (ABM) alone, the composite of ABM with P15 protein (ABM/P15) possessed good biocompatibility and exhibited superior bone regeneration efficacy in promoting the repair of periodontal bone defects in rats, achieving better periodontal tissue restoration and greater bone regeneration height. The experiments demonstrated that ABM/P15 did not induce significant elevations in the levels of key apoptotic proteins (Caspase-3 and Bcl-2), suggesting that its mechanism for promoting regeneration might be related to enhancing fibroblast migration and adhesion rather than significantly altering the apoptotic pathways examined. This study laid an experimental foundation for the clinical application of ABM/P15, and its "material-structure-function" collaborative design concept made it possible for periodontal regenerative medicine to change from standardized to intelligent diagnosis and treatment mode.

Statement: All authors have no conflicts of interest.

Animal rights statement: All animal experiments were approved by the Animal Ethics Committee of Hunan University of Chinese Medicine Affiliated Changsha Stomatological Hospital, and in accordance with the Guide for the Care and Use of Laboratory Animals published by the United States National Institutes of Health.

Authors' Contributions: Wenhua Xu and Xiaoliang Luo designed experiments; Lifen Yin and Meilu Zhou collected and analyzed data; Wenhua Xu and Xiaoliang Luo performed experiments; Wenhua Xu and Xiaoliang Luo wrote the manuscript. All authors agreed to publish this article.

REFERENCES

Akindoyo, J.O., S. Ghazali, M.D.H. Beg, and N. Jeyaratnam (2019). Characterization and elemental quantification of natural hydroxyapatite produced from cow bone. Chem Eng Technol. 42(9): 1805-1815. https://doi.org/10.1002/ceat.201800636

Amelot, A., A. Nataloni, P. François, A.R. Cook, J.P. Lejeune, M. Baroncini, P.L. Hénaux, P. Toussaint, J. Peltier, K. Buffenoir, O. Hamel, P.D. Hieu, S. Chibbaro, P. Kehrli, M.A. Lahlou, P. Menei, M. Lonjon, C. Mottolese, P. Peruzzi, K. Mahla, D. Scarvada, C. Le Guerinel, P. Caillaud, C. Nuti, B. Pommier, T. Faillot, G. Iakovlev, S. Goutagny, N. Lonjon, P. Cornu, P. Bousquet, P. Sabatier, B. Debono, J.P. Lescure, E. Vicaut, and S. Froelich (2021). Security and reliability of CUSTOMBONE cranioplasties: A prospective multicentric study. Neurochirurgie. 67(4): 301–309. https://doi.org/10.1016/j.neuchi.2021.02.007

Andresen, A.K., L.Y. Carreon, S. Overgaard, M.K. Jacobsen, and M.Ø. Andersen (2022). Safety and Reoperation Rates in Non-Instrumented Lumbar Fusion Surgery: Secondary Report From a Randomized Controlled Trial of ABM/P-15 vs Allograft With Minimum 5 years Follow-Up. Global Spine J. 14(1): 33-40. https://doi.org/10.1177/21925682221090924

Atieh, M.A., N.H. Alsabeeha, A.G. Payne, S. Ali, C.M.J. Faggion, and M. Esposito (2021). Interventions for replacing missing teeth: alveolar ridge preservation techniques for dental implant site development. Cochrane Database Syst Rev. 4(4): CD010176. https://doi.org/10.1002/14651858.CD010176.pub3

Axelsen, M. G., S. Overgaard, S. M. Jespersen, and M. Ding (2019). Comparison of synthetic bone graft ABM/P-15 and allograft on uninstrumented posterior lumbar spine fusion in sheep. J Orthop Surg Res. 14(1): 2. https://doi.org/10.1186/s13018-018-1042-4

Babayiğit, O., E. Öncü, G. Mağat, and K. Orhan (2023). Effect of Maxillary Sinus Anatomy on Bone Gain After Lateral Window Sinus Floor Elevation: A Case-Control Study. Int J Oral Maxillofac Implants. 38(2): 338–346. https://doi.org/10.11607/jomi.9980

Badaro-Garcia, S., M.S. Hohmann, A.L. Coelho, W.A. Verri Jr, and C.M. Hogaboam (2023). Standard of care drugs do not modulate activity of senescent primary human lung fibroblasts. Sci Rep. 13(1): 3654. https://doi.org/10.1038/s41598-023-30844-0

Bergara-Muguruza, L., K. Mäkelä, T. Yrjälä, J. Salonen, K. Yamashita, and M. Nakamura (2021). Surface Electric Fields Increase Human Osteoclast Resorption through Improved Wettability on Carbonate-Incorporated Apatite. ACS Appl Mater Interfaces. 13(49): 58270–58278. https://doi.org/10.1021/acsami.1c14358

Budiatin, A. S., J. Khotib, S. Samirah, C. Ardianto, M. A. Gani, B. R. K. H. Putri, H. Arofik, R. N. Sadiwa, I. Lestari, Y. A. Pratama, E. Rahadiansyah, and I. Susilo (2022). Acceleration of Bone Fracture Healing through the Use of Bovine Hydroxyapatite or Calcium Lactate Oral and Implant Bovine Hydroxyapatite-Gelatin on Bone Defect Animal Model. Polymers. 14(22): 4812. https://doi.org/10.3390/polym14224812

Chan, L.Y., J. Du, and D.J. Craik (2021). Tuning the Anti-Angiogenic Effect of the P15 Peptide Using Cyclic Trypsin Inhibitor Scaffolds. ACS Chem Biol. 16(5): 829–837. https://doi.org/10.1021/acschembio.0c00907

Chang, Y.T., C.C. Lai, and D.J. Lin (2023). Collagen Scaffolds Laden with Human Periodontal Ligament Fibroblasts Promote Periodontal Regeneration in SD Rat Model. Polymers (Basel). 15(12): 2649. https://doi.org/10.3390/polym15122649

Chen, E., T. Wang, Z. Sun, Z. Gu, S. Xiao and Y. Ding (2024). Polyphenols-based intelligent oral barrier membranes for periodontal bone defect reconstruction. Regen Biomater. 11: rbae058. https://doi.org/10.1093/rb/rbae058

Chiu, Y. L., Y. L. Luo, Y. W. Chen, C. T. Wu, S. Periasamy, K. C. Yen, and D. J. Hsieh (2022). Regenerative Efficacy of Supercritical Carbon Dioxide-Derived Bone Graft Putty in Rabbit Bone Defect Model. Biomedicines. 10(11): 2802. https://doi.org/10.3390/biomedicines10112802

Costa, M. R., J. A. C. Filho, C. B. B. Luna, G. M. P. Dantas, A. C. F. M. Costa, and N. M. D. S. Oliveira (2024). Toward the Production of Hydroxyapatite/Poly(Ether-Ether-Ketone) (PEEK) Biocomposites: Exploring the Physicochemical, Mechanical, Cytotoxic and Antimicrobial Properties. Polymers (Basel). 16(17): 2520. https://doi.org/10.3390/polym16172520

Diansari, V., R. Idroes, S. Sunarso, and S. Fitriyani (2025). Extraction and Characterization of Aceh Bovine Bone-Derived Hydroxyapatite for Applications in Dentistry. Eur J Dent. 19(4): 1169-1178. https://doi.org/10.1055/s-0045-1802946

Elabbasy, M.T., M.H. Alshammari, R. Zrieq, R.M. El Bayomi, A.B.M.B. Tahoun, M.A. El-Morsy, and M.F.H. Abd El-Kader (2023). Physical and biological changes of copper oxide and hydroxyapatite filled in polycaprolactone scaffolds: Cellular growth behavior and antibacterial activity. J Mech Behav Biomed Mater. 144: 105927. https://doi.org/10.1016/j.jmbbm.2023.105927

Elfana, A.M., and M.T. Elbehwashy (2022). Periodontal regeneration using connective tissue graft wall and xenograft with coronally advanced flap in noncontained intrabony defects: A novel combination technique. J Indian Soc Periodontol. 26(3): 295–298. https://doi.org/10.4103/jisp.jisp_347_21

Elgendy, E.A., A.M. Elgendy, and O.M. ElBorady (2023). Clinical And Radiographic Assessment of Autogenous Dentin Nanoparticles in Treatment of Stage Iii Periodontitis: A Split-Mouth Clinical Study. J Pak Med Assoc. 73(Suppl 4) (4): S310–S316. https://doi.org/10.47391/JPMA.EGY-S4-60

Gani, A., R. Yulianty, S. Supiaty, M. Rusdy, G. Dwipa Asri, D. Eka Satya, A. Rahayu Feblina, and H. Achmad (2022). Effectiveness of Combination of Chitosan Gel and Hydroxyapatite from Crabs Shells (Portunus pelagicus) Waste as Bonegraft on Periodontal Network Regeneration through IL-1 and BMP-2 Analysis. Int J Biomater. 2022: 1817236. https://doi.org/10.1155/2022/1817236

Grün, P., F. Pfaffeneder-Mantai, P. Bandura, B. Schneider, U. Degel, A.S. Grün, and D. Turhani (2023). Bone remodeling of the sinus floor observed 19 years after third molar transplantation to close a maxillary defect: a case report. Ann Med Surg (Lond). 85(5): 1991–1997. https://doi.org/10.1097/MS9.0000000000000475

Guo, P., D. Wang, S. Zhang, D. Cheng, S. Wu, X. Zuo, Y.B. Jiang, and T. Jiang (2023). Reassembly of Peptide Nanofibrils on Live Cell Surfaces Promotes Cell-Cell Interactions. Nano Lett. 23(14): 6386–6392. https://doi.org/10.1021/acs.nanolett.3c01100

Iqbal, B., Z. Sarfaraz, N. Muhammad, P. Ahmad, J. Iqbal, Z.U.H. Khan, G. Gonfa, F. Iqbal, A. Jamal, and A. Rahim (2018). Ionic liquid as a potential solvent for preparation of collagen-alginate-hydroxyapatite beads as bone filler. J Biomater Sci Polym Ed. 29(10): 1168–1184. https://doi.org/10.1080/09205063.2018.1443604

Jacobsen, M.K., A.K. Andresen, A.B. Jespersen, C. Støttrup, L.Y. Carreon, S. Overgaard, and M.Ø. Andersen (2020). Randomized double blind clinical trial of ABM/P-15 versus allograft in noninstrumented lumbar fusion surgery. Spine J. 20(5): 677–684. https://doi.org/10.1016/j.spinee.2020.01.009

Jann, J., O. Drevelle, M.A. Lauzon, and N. Faucheux (2020). Adhesion, intracellular signalling and osteogenic differentiation of mesenchymal progenitor cells and preosteoblasts on poly(epsilon)caprolactone films functionalized by peptides derived from fibronectin and/or BMP-9. Mater Sci Eng C Mater Biol Appl. 114: 111088. https://doi.org/10.1016/j.msec.2020.111088

Klassmann, F.A., E. Ervolino, L.E. Kluppel, L.H. Theodoro, G. Mulinari-Santos, and V.G. Garcia (2023). A randomised trial of the bone formation after maxillary sinus floor augmentation with bovine hydroxyapatite (Cerabone®) and Photobiomodulation: histomorphometric and immunohistochemical analysis. J Clin Exp Dent. 15(7): e542–e550. https://doi.org/10.4317/jced.60594

Li, Y., J. Nie, C. Deng, and H. Li (2023). P-15 promotes chondrocyte proliferation in osteoarthritis by regulating SFPQ to target the Akt-RUNX2 axis. J Orthop Surg Res. 18(1): 199. https://doi.org/10.1186/s13018-023-03658-z

Loenen, A.C.Y., J. Connor, S. Johnson, K. Davis, N. Hannigan, T. Barnes, J.J. Arts, and B. van Rietbergen (2022). Peptide Enhanced Bone Graft Substitute Presents Improved Short-Term Increase in Bone Volume and Construct Stiffness Compared to Iliac Crest Autologous Bone in an Ovine Lumbar Interbody Fusion Model. Global Spine J. 12(7): 1330–1337. https://doi.org/10.1177/2192568220979839

Minim, P.R., L.J. de Azevedo-Silva, B.M. Ferrairo, L.F. Pereira, C.A. Goulart, R.S. Monteiro-Sousa, P.N. Lisboa Filho, C.A. Fortulan, R. Salomão, A.F.S. Borges, and J.H. Rubo (2023). The combined effects of binder addition and different sintering methods on the mechanical properties of bovine hydroxyapatite. J Mech Behav Biomed Mater. 144: 105993. https://doi.org/10.1016/j.jmbbm.2023.105993

Mishra, P.R.N., A.P. Kolte, R.A. Kolte, N.G. Pajnigara, and K.K. Shah (2019). Comparative evaluation of open flap debridement alone and in combination with anorganic bone matrix/cell-binding peptide in the treatment of human infrabony defects: A randomized clinical trial. J Indian Soc Periodontol. 23(1): 42–47. https://doi.org/10.4103/jisp.jisp_339_18

Mohanram, Y., J. Zhang, E. Tsiridis, and X.B. Yang (2020). Comparing bone tissue engineering efficacy of HDPSCs, HBMSCs on 3D biomimetic ABM-P-15 scaffolds in vitro and in vivo. Cytotechnology. 72(5): 715–730. https://doi.org/10.1007/s10616-020-00414-7

Özer, T., V. Guliyeva, A. Aktaş, E. Barış, and M. Ocak (2023). Effects of a locally administered risedronate/autogenous bone graft combination on bone healing in a critical-size rabbit defect model. J Orthop Surg Res. 18(1): 88. https://doi.org/10.1186/s13018-023-03568-0

Ratnayake, J., N. Ramesh, M. L. Gould, M. R. Mucalo, and G. J. Dias (2025). Silicate-substituted bovine-derived hydroxyapatite as a bone substitute in regenerative dentistry. J Appl Biomater Funct Mater. 23: 22808000251314302. https://doi.org/10.1177/22808000251314302

Sah, N., P. P. Sarode, A. Warang, T. Tarase, P. Gavhale, and M. Mirgane (2025). Alveolar Ridge Preservation Using Xenograft Following Tooth Extraction: A Systematic Review and Meta-Analysis. Cureus. 17(4): e81815. https://doi.org/10.7759/cureus.81815

Shaikh, M.S., S. Husain, M.A. Lone, M.A. Lone, H. Akhlaq, and M.S. Zafar (2020). Clinical effectiveness of anorganic bovine-derived hydroxyapatite matrix/cell-binding peptide grafts for regeneration of periodontal defects: a systematic review and meta-analysis. Regen Med. 15(12): 2379–2395. https://doi.org/10.2217/rme-2020-0113

Sindhusha, V. B. and J. N. Doraiswamy (2024). The Role of Chitosan and Gelatin-Based Scaffolds in Bone Regeneration: A Systematic Review. Cureus. 16(9): e69793. https://doi.org/10.7759/cureus.69793

Ureiro-Cueto, G., S. E. Rodil, M. Santana-Vázquez, L. Hoz-Rodriguez, H. Arzate and G. Montoya-Ayala (2024). Characterization of aTiO2 surfaces functionalized with CAP-p15 peptide. J Biomed Mater Res A. 112(9): 1399–1411. https://doi.org/10.1002/jbm.a.37676

Venkataiah, V.S., K. Handa, M.M. Njuguna, T. Hasegawa, K. Maruyama, E. Nemoto, S. Yamada, S. Sugawara, L. Lu, M. Takedachi, S. Murakami, H. Okura, A. Matsuyama, and M. Saito (2019). Periodontal Regeneration by Allogeneic Transplantation of Adipose Tissue Derived Multi-Lineage Progenitor Stem Cells in vivo. Sci Rep. 9(1): 921. https://doi.org/10.1038/s41598-018-37528-0

Wang, M., L. Zhang, F. Lin, Q. Zheng, X. Xu, and L. Mei (2021). Dynamic study into autophagy and apoptosis during orthodontic tooth movement. Exp Ther Med. 21(5): 430. https://doi.org/10.3892/etm.2021.9847

Wang, X., W. Chen, Z. Chen, Y. Li, K. Wu, and Y. Song (2022). Preparation of 3D Printing PLGA Scaffold with BMP-9 and P-15 Peptide Hydrogel and Its Application in the Treatment of Bone Defects in Rabbits. Contrast Media Mol Imaging. 2022: 1081957. https://doi.org/10.1155/2022/1081957

Xu, X., Z. Chen, L. Xiao, Y. Xu, N. Xiao, W. Jin, Y. Chen, Y. Li, and K. Luo (2023). Nanosilicate-functionalized nanofibrous membrane facilitated periodontal regeneration potential by harnessing periodontal ligament cell-mediated osteogenesis and immunomodulation. J Nanobiotechnology. 21(1): 223. https://doi.org/10.1186/s12951-023-01982-4

Yang, J., J. Su, Z. Sun, Y. Song, Y. Zhang, Z. Zhang, J. Wei, X. Shi, N. Jiang, and X. Ge (2024). Youthful small extracellular vesicles restore the function and reparative capacity of inflammatory-impaired periodontal ligament stem cells via delivering protein biglycan for bone regeneration. J Nanobiotechnology. 22(1): 508. https://doi.org/10.1186/s12951-024-02752-6

Yang, W., S. Yu, J. Peng, P. Chang, and X. Chen (2023). FGF12 regulates cell cycle gene expression and promotes follicular granulosa cell proliferation through ERK phosphorylation in geese. Poult Sci. 102(10): 102937. https://doi.org/10.1016/j.psj.2023.102937

Yao, S., Y. Shang, B. Ren, S. Deng, Z. Wang, Y. Peng, Z. Huang, S. Ma, C. Peng, and S. Hou (2022). A novel natural-derived tilapia skin collagen mineralized with hydroxyapatite as a potential bone-grafting scaffold. J Biomater Appl. 37(2): 219–237. https://doi.org/10.1177/08853282221086246

Yukna, R.A., J.T. Krauser, D.P. Callan, G.H. Evans, R. Cruz, and M. Martin (2000). Multi-center clinical comparison of combination anorganic bovine-derived hydroxyapatite matrix (ABM)/cell binding peptide (P-15) and ABM in human periodontal osseous defects. 6-month results. J Periodontol. 71(11): 1671–1679. https://doi.org/10.1902/jop.2000.71.11.1671

Zhang, J., P. Eisenhauer, O. Kaya, A.R. Vaccaro, C. Diallo, A. Fertala, and T.A. Freeman (2017). P15 peptide stimulates chondrogenic commitment and endochondral ossification. Int Orthop. 41(7): 1413–1422. https://doi.org/10.1007/s00264-017-3464-8

Zhang, Y., J. Ren, Z. Shen, J. Yang, J. Yang, Z. Lin, X. Shi, C. Zhao and J. Xia (2025) BMP2 peptide-modified polycaprolactone-collagen nanosheets for periodontal tissue regeneration. Front Bioeng Biotechnol. 13: 1523735. https://doi.org/10.3389/fbioe.2025.1523735